

Supporting Information-Molecular Dynamics of Polymyrcene: Rheology and Broadband Dielectric Spectroscopy on a Stockmayer Type A Polymer

Ciprian Iacob,^{*,†,‡} Matthias Heck,^{*,†} and Manfred Wilhelm^{*,†}

*†Institute for Chemical Technology and Polymer Chemistry, Karlsruhe Institute of Technology,
76131 Karlsruhe, Germany*

*‡National Research and Development Institute for Cryogenic and Isotopic Technologies, 240050
Rm. Valcea, Romania*

E-mail: Ciprian.Iacob@kit.edu; Matthias.Heck@kit.edu; Manfred.Wilhelm@kit.edu

Author Information

Corresponding Authors:

*E-mail: Ciprian.Iacob@kit.edu
*E-mail: Matthias.Heck@kit.edu
*E-mail: Manfred.Wilhelm@kit.edu

Orcid

Ciprian Iacob [0000-0001-7982-0586](https://orcid.org/0000-0001-7982-0586)
Matthias Heck [0000-0002-7752-1838](https://orcid.org/0000-0002-7752-1838)
Manfred Wilhelm [0000-0003-2105-6946](https://orcid.org/0000-0003-2105-6946)

Chemical Structures

The chemical structures of the terpene isoprene and the sesquiterpenes myrcene and β -farnesene as well as their respective polymers are displayed in Figure 1. The polymer polymyrcene (PM) was synthesized in this study. The polymers polyisoprene (PI) and polyfarnesene (PF) are displayed as comparison. The size of the pendant groups of PM (C6 for the 1,4-addition product; C8 for the 3,4-addition product) are in between the ones of PI (C1 for the 1,4-addition product; C3 for the 3,4-addition product) and PF (C11 for the 1,4-addition product; C13 for the 3,4-addition product).

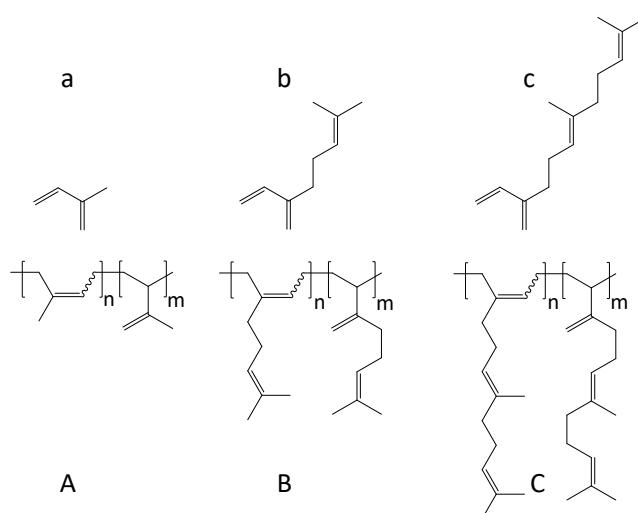


Figure 1: Chemical structure of the monomers (upper row) and their respective polymers (lower row), which were compared in this study. Monomers: (a) isoprene, (b) myrcene and (c) β -farnesene. Polymers: (A) Polyisoprene, (B) Polymyrcene and (C) Polyfarnesene. The structures of the 1,4-(*cis* and *trans*)-addition products are displayed in the brackets labeled with n (depending if the undulated bond is *cis* or *trans* to the other backbone bond) and the 3,4-addition products in the brackets labeled with m.

Isomer Content

The relative isomer content Φ of the individual PM samples was calculated from the integrals in an $^1\text{H-NMR}$ spectrum as displayed in Figure 3 of the article. A Bruker Avance III Microbay 400 MHz spectrometer was used and 512 scans were performed per measurement. The integrals at 4.77 & 4.81 ppm (just 3,4-PM) and 1.56 & 1.67 ppm (3,4-PM + 1,4-PM) were used for the determination

of the isomer content. The 1,4-isomer could not further be discriminated into *cis*-1,4-PM and *trans*-1,4-PM due to the field strength. The isomer contents calculated from the peak integrals are summarized in Table 1.

Table 1: Isomer contents determined by 400 MHz $^1\text{H-NMR}$ (512 scans) in CDCl_3 .

sample ID	$\Phi_{3,4}$ (%)	$\Phi_{1,4}$ (%)
PM6.7	6.25	93.75
PM11.6	5.61	94.39
PM14.8	6.08	93.92
PM36.6	7.75	92.25
PM42.1	7.82	92.18
PM74.1	6.31	93.69
PM85.6	5.78	94.22
PM115.5	6.16	93.84
PM155.1	6.75	93.25
PM192	7.24	92.76
PM347.7	5.82	94.18

Vogel-Fulcher-Tamman-Fit

The Fitting parameters obtained by the Vogel-Fucher-Tamman-Fit (VFT; Equation 5 in the article) for all individual samples are summarized in Table 2.

Table 2: Fitting-parameters obtained by the Vogel-Fucher-Tamman-Fit (VFT) for the normal mode- and α -segmental relaxations of the PM samples.

sample ID	$\omega_{n'}/\omega_{\alpha'}$ (s^{-1})	$B_{n'}/B_{\alpha'}$ (K)	$T_{0n'}/T_{\alpha'}$ (K)
PM6.7	3.21e8/8.7e8	7.8/3.03	161.7/185
PM11.6	1.28e8/8.1e8	8.6/3.34	158.8/181.3
PM14.8	6.4e7/6.6e8	8.2/3.89	160.6/179.4
PM36.6	1.27e8/7.8e8	8.6/3.91	158.8/178.6
PM42.1	3.45e6/4.21e8	8.17/3.32	163.3/179.3
PM74.1	1.16e6/8.12e8	8.23/3.56	164.2/180.3
PM85.6	5.7e5/4.27e9	7.93/4.00	163.6/178
PM115.5	2.08e5/8.7e8	7.84/3.05	164.5/181.6
PM155.1	3.9e4/5.42e8	8.67/3.05	160.9/179.3
PM192	9e5/1.66e8	8.51/3.15	162.5/180.3
PM347.7	8.8e5/2.34e8	8.53/3.24	163.1/183.7

Density

The density of the individual PM samples was determined as described in the article. The value for each sample is listed in Table 3.

Table 3: Density values determined for each of the PM samples.

sample ID	Density (g/cm ³)
PM6.7	0.89
PM10.7	0.89
PM11.6	0.90
PM20.9	0.89
PM36.6	0.91
PM42.1	0.91
PM74.1	0.91
PM85.6	0.91
PM115.5	0.91
PM155.1	0.91
PM192	0.91
PM347.7	0.91

Relaxation Times

The determination of the chain and segmental relaxation times is demonstrated for one PM sample in Figure 2 a. In the dielectrical master curve (upper graph), the relaxation times can be determined by the maxima of M'' . In the mechanical master curve (lower graph), the relaxation times can be determined by the crossing of the storage G' and loss modulus G'' .

In order to compare results obtained by the two techniques, mechanical and dielectric, and in order to avoid any controversy regarding the characteristic times determined from various representations of data and any possible uncertainties, we are going to compare the imaginary part of the complex modulus, M'' (directly related to relaxation rate) with G' and G'' for a representative PM sample (PM115.9 kg/mol) at reference temperature as indicated. The dielectric modulus M'' shows a similar behavior (two peaks corresponding to chain relaxation and segmental relaxation respectively) that corresponds to the mechanical segmental relaxation time ($\tau_c = 1/\omega_c$) at T_{ref} . The

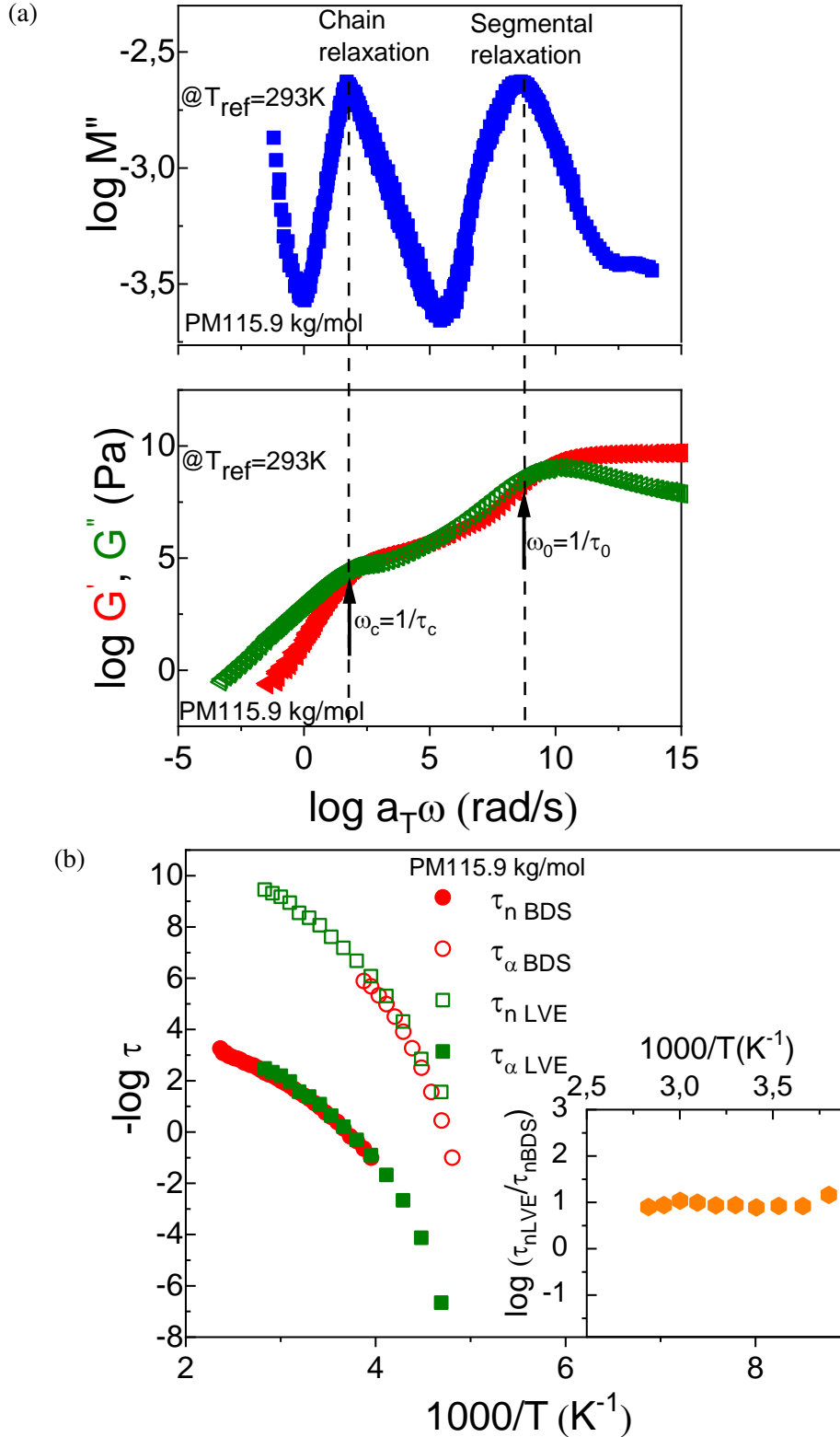


Figure 2: (a) Depiction of electrical and mechanical master curves for PM115.9 ($M_w = 115.9$ kg/mol). The vertical dashed lines indicate the position of the M'' maxima. (b) Temperature dependence of the segmental and chain relaxation times determined from dielectric spectra and chain relaxation from mechanical spectra for PM. Insets: The ratio of viscoelastic relaxation time to dielectric relaxation time.

segmental relaxation time τ_c is obtained at the frequency ω_c , at the transition between the Newtonian flow range at low frequencies and the rubbery range at high frequencies at which the storage G' and the loss G'' moduli cross each other and $(\tau_0 = 1/\omega_0)$ at T_{ref} is obtained at the frequency ω_0 , in the glassy state region. At high frequency, a well-defined rubbery plateau is apparent in the PM sample. As frequency decreases, the material transitions from a well-defined rubbery plateau to the crossover of G' and G'' , ending in a smooth transition to the terminal region. The presence of the distinct rubber plateau in PM115.9 indicates the presence of entanglements. In order to quantify the differences between chain relaxation from BDS and LVE in Figure 2 we analyzed an entangled PM sample where we demonstrated that there is a good coincidence of the terminal relaxation times obtained from LVE measurements and normal-mode relaxation times obtained from dielectric spectroscopy.

In order to quantify the agreement of the data describing the molecular dynamics of PM obtained by BDS and LVE, the relaxation times determined with both techniques were compared. The viscoelastic and dielectric relaxation times are plotted versus the inverse temperature in Figure 2 b. The relaxation time ($\tau_{n,LVE}$) corresponding to the transition between the Newtonian flow range at low frequencies and the rubbery plateau range at higher frequencies was determined as $\tau(T_{ref}) = 1/\omega_c$, where ω_c is the frequency at which G' and G'' cross each other. The results show a good coincidence of the terminal relaxation times obtained from LVE measurements and the normal-mode relaxation times obtained from dielectric spectroscopy as displayed in Figure 2 b. Even though the results from LVE and BDS overlap only within a relatively narrow temperature range (related to a narrow window of the determined normal mode), they can be represented as a ratio which is approaching unity, which is displayed in the inset of Figure 2 b.

Entanglements

The polycarbonate samples used in this study cover a molecular weight from below their entanglement molecular weight M_e to molecular weights far beyond M_e . The crossing of the storage G' and the

loss moduli G'' in the sample's mastercurves was used as a criteria to distinguish between entangled and unentangled PM samples. In order to make the separation of the samples more clearly, the master curves of the two samples at the border of critical molecular weight of M_c are compared in Figure 3 (b). The van Gulp–Palmen plot is also constructed in order to show that TTS can be applied from terminal regime to the glassy state.

Time-Temperature-Superposition and Glass Transition Temperature

Master curves describing the frequency dependence of the polymer melt were generated by frequency-scale shifting the isothermal frequency sweep data, within the linear regime, from 393 K to 213 K (with increments of 10 K) for all PM samples. Time-temperature superposition (TTS) works well (for the temperatures above T_g) for the LVE spectra and the segmental relaxation is confirmed to be associated with the α -process observed in BDS by fitting the temperature dependence of the frequency-scale horizontal shift factors (a_T) with the WLF equation. A master curve, which includes data obtained at temperatures below T_g is displayed in Figure 4. The T_g was obtained from the local maximum of G'' from the master curves that corresponds to the crossover of the shift factors where the application of TTS fails. To approximate a frequency independent T_g , the data was shifted to a low angular frequency such as 0.01 rad/s. The failing of TTS is exhibited by the transition of the WLF behavior of the frequency shift factors a_T to an Arrhenius behavior at T_g (see inset of Figure 4). Due to the inapplicability of TTS beyond a phase transition the shifted data has to be considered with caution. At the high frequencies of the shifted data, additional processes would normally occur, but could not be observed, because the measured frequencies were much too low to do so. Thus the data in the gray box of Figure 4 does not represent reality and is not in the main article, but still helps to illustrate the failing of TTS around T_g .

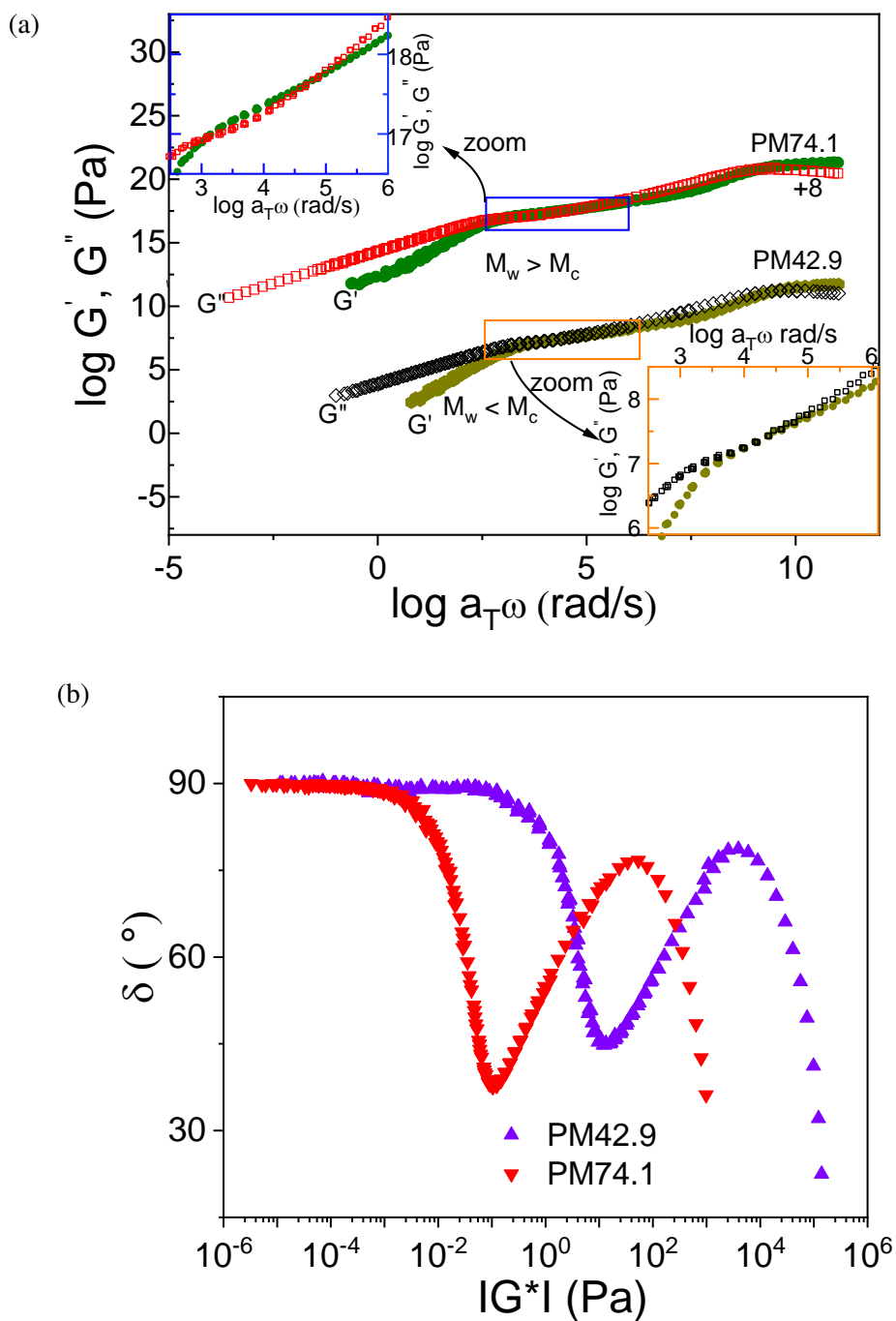


Figure 3: Dynamic master curves of the storage and loss moduli for the PM samples PM42.9 and PM74.1 at a reference temperature of $T_{ref} = 293$ K. The curve of PM74.1 is shifted vertically using the indicated vertical scale factor of 8. For the sample PM42.9 the moduli G' and G'' approach, but never cross each other, thus this sample is considered as unentangled. However, for PM74.1 the two moduli cross each other, thus this sample is considered as entangled and (b) van Gurp-Palmen plot of PM42.9 and PM74.1 constructed using the data of master curves presented in (a).

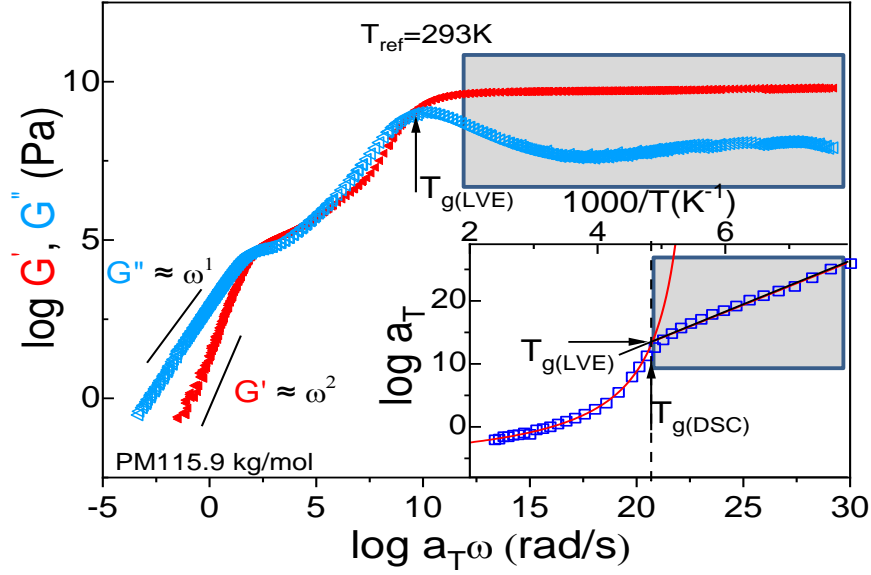


Figure 4: Storage and loss modulus of PM115.9 at $T_{ref} = 293$ K from the terminal regime to the glassy state. Inset: Horizontal shift factor a_T used to generate the master curve. The deviation of the shift factor a_T from VFT clearly demonstrate the breakdown of time-temperature superposition below T_g . The solid red line represents fits using the WLF equation. The dashed vertical line represents the glass transition temperature obtained by DSC and LVE measurements. The glass transition from LVE is also indicated by the crossover of the shift factors that corresponds to the measured temperature of the local maximum of G'' from the mastercurves as indicated. Data, which was obtained at measurements below T_g and was shifted using TTS (gray box) has to be considered with caution.

Comparison of PI, PM and PF

The ratio τ_n/τ_α of the normal mode τ_n and the α -relaxation time τ_α as a function of the molecular weight M_w of three polyterpenes PI, PM and PF and as a function of M_w/M_c is compared in the main article. In Figure 5 the molecular weight M_w is normalized to the entanglement molecular weights of the respective polymer M_e and this ratio is displayed as a function of entanglements Z .

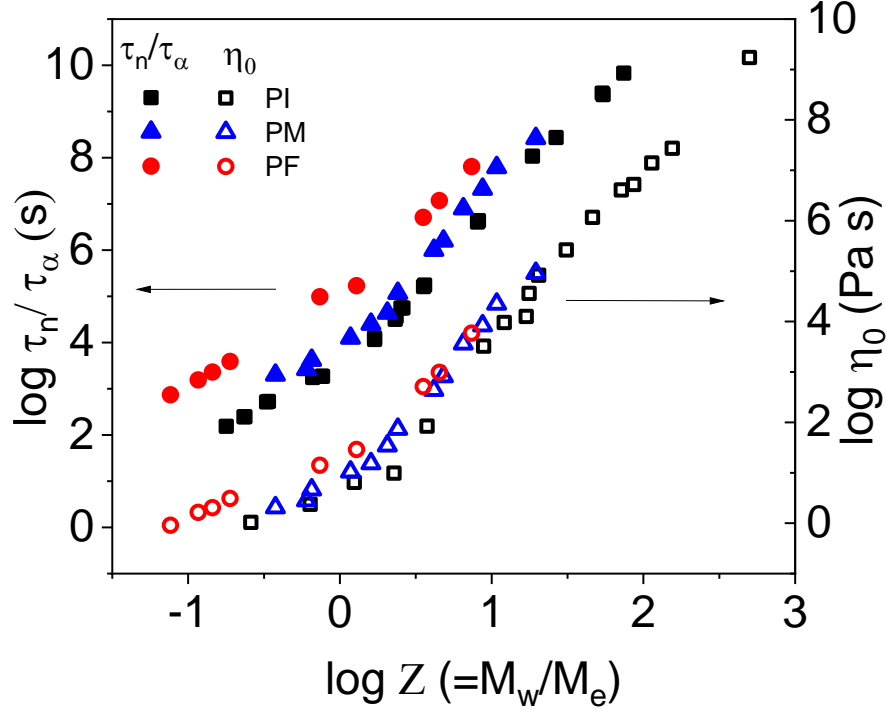


Figure 5: Solid symbols: Dielectric normal mode relaxation times for polyisoprene (PI- square-symbols),¹⁻³ polyfarnesene (PF-circle symbols-)⁴ and polymyrcene (PM-triangle symbol) versus Z -the number of entanglements at an iso-frictional state. Open symbols: Zero shear viscosities at $T = 293$ K as a function of Z for the PI,⁵ PF⁴ and PM materials.

Experimental Setup

The rheological experiments were conducted at a rheo-dielectric setup at KIT. Broadband dielectric measurements were conducted either with a dedicated dielectric setup at ICSI Energy department or the rheo-dielectric setup at KIT. Both setups are shown in Figure 6. With the rheo-dielectric combination it is possible to do rheological and BDS measurements at the same time. However, in this study these experiments were conducted separately to avoid any possible influence to each other.

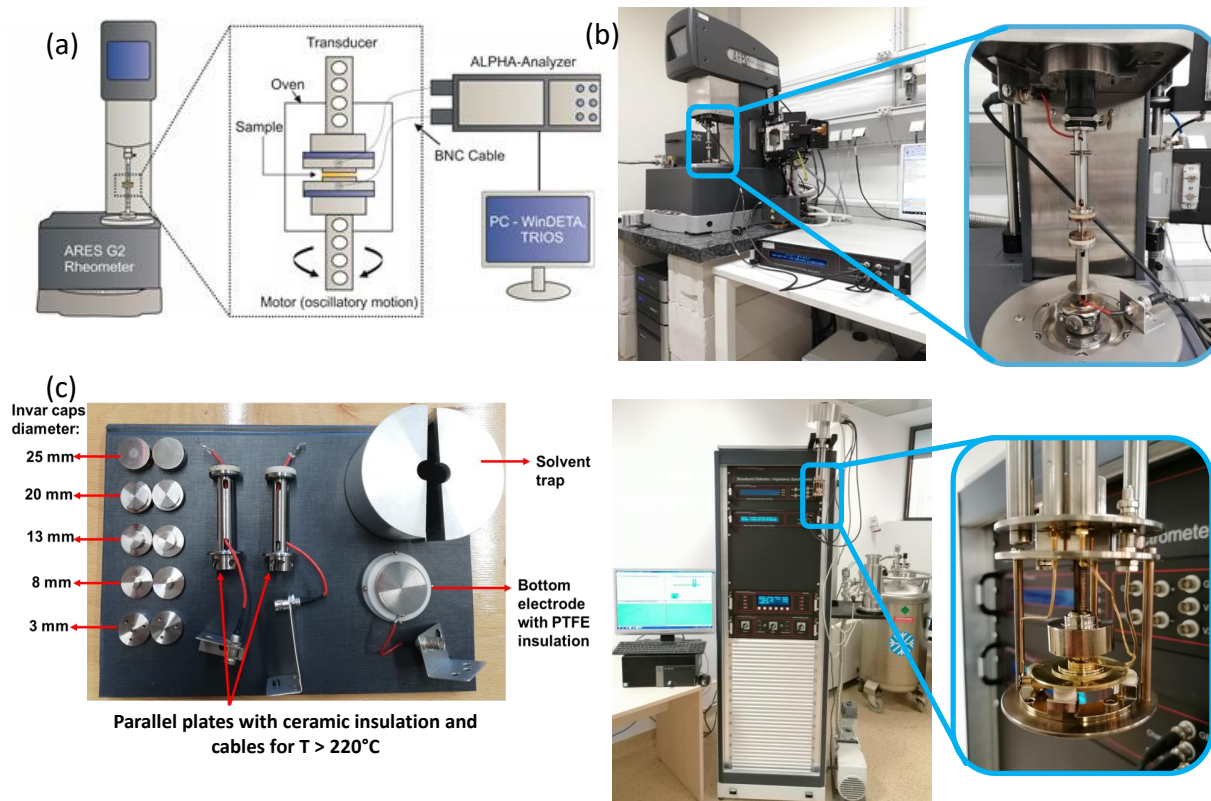


Figure 6: (a) Scheme of the rheo-dielectrics setup, (b) coupled rheo-dielectrics setup - ARES G2 from TA Instruments coupled to an Alpha analyzer from Novocontrol- available at KIT in the group of Prof. Manfred Wilhelm, (c) parallel plates with different diameters with ceramic insulation and cables for high temperatures measurements, solvent trap with bottom electrode with PTFE insulation for measurements with a Peltier temperature control setup-available at KIT in the group of Prof. Manfred Wilhelm and (d) Alpha analyzer Concept 40 with Quattro Cryosystem temperature controller and Alpha active measurement cell from Novocontrol available at ICSI Energy department at ICSI Rm. Valcea.

Enlarged Figures of the Main Document

For a better readability all the figures of the article are displayed in an enlarged version in this section.

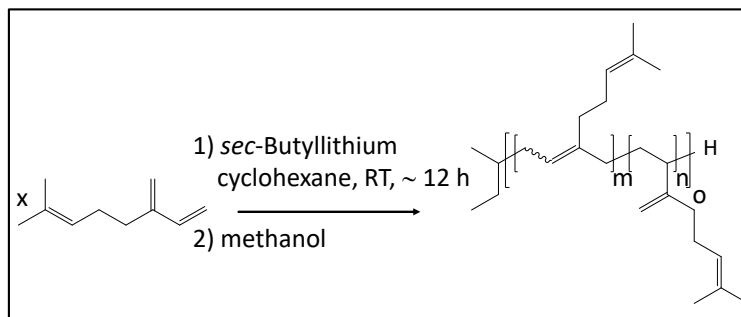


Figure 7: Anionic polymerization of myrcene in cyclohexane using *sec*-BuLi as an initiator. Under these experimental conditions more than 90 mol% of the 1,4-isomer was obtained (determined by $^1\text{H-NMR}$).

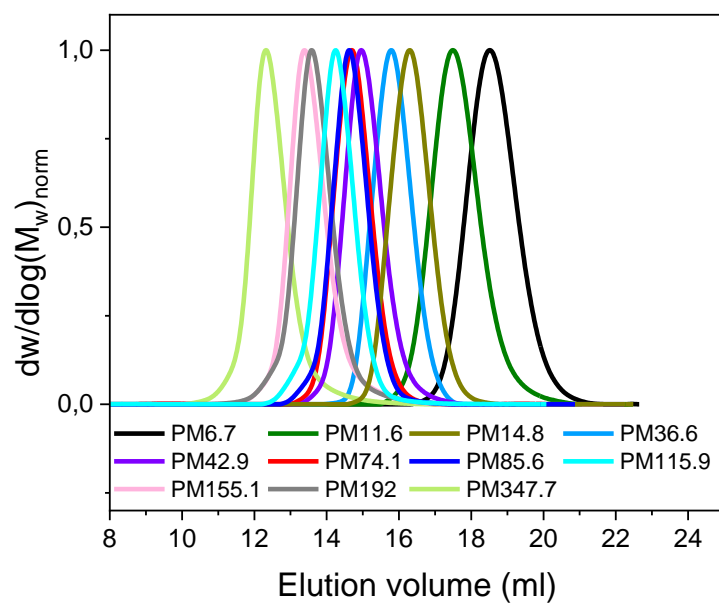


Figure 8: Normalized SEC traces for the PM samples versus the elution volume. The SEC traces determined by the DRI detector are displayed.

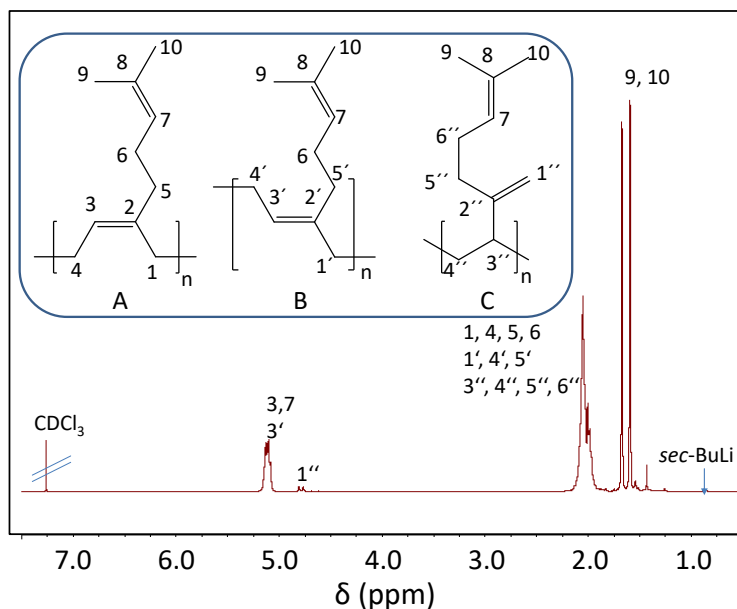


Figure 9: 400 MHz ^1H -NMR spectrum of PM in CDCl_3 (512 scans). Inset: Structure of *cis*-1,4-PM (A), *trans*-1,4-PM (B) and 3,4-PM (C).⁶

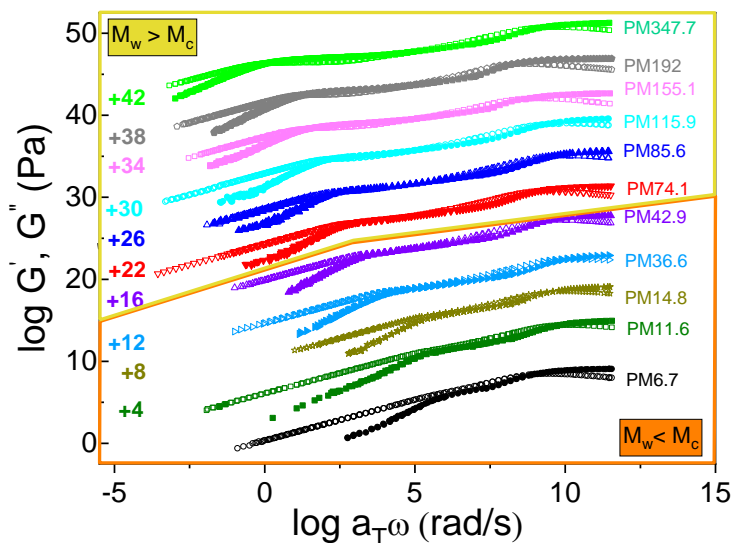


Figure 10: Dynamic rheological master curves of the storage and loss moduli for all PM samples from the terminal region to the glassy state at a reference temperature of $T_{ref} = 293$ K. The curves were shifted vertically. The scale factors are listed at the left side of the y-axis. The molecular weights of the PM polymers below and above critical molecular weight M_c are also indicated by the line between PM42.9 and PM74.1. The crossing of the storage G' and the loss moduli G'' , from the terminal region to the rubber plateau, in the sample's mastercurves was used as a criteria to distinguish between entangled and unentangled PM samples. In order to make the separation of the samples more clearly, the master curves of the two samples (PM42.9 and PM74.1) at the border of critical molecular weight of M_c are compared in Figure 3, SI.

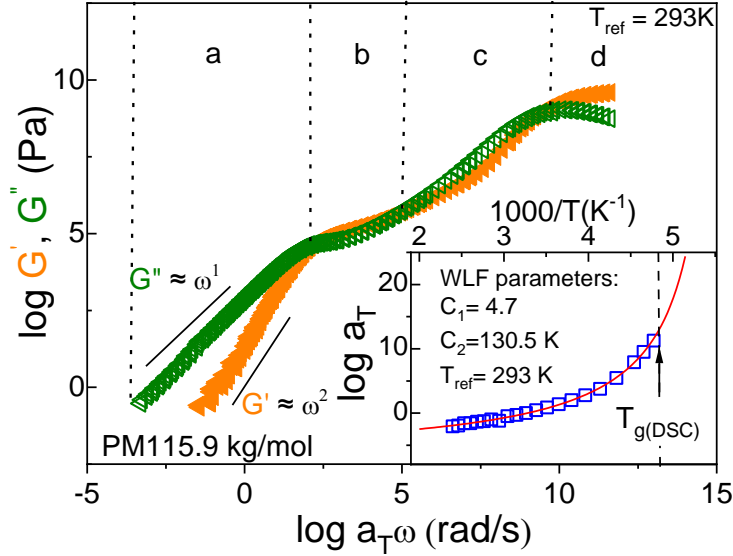


Figure 11: Storage and loss modulus of PM115.9 at $T_{ref} = 293$ K from the terminal regime (a) via the rubber plateau (b) and the transition zone (c) to the glassy state (d). Inset: Horizontal shift factor a_T used to generate the master curve. The solid red line represents fits using the WLF equation. The dashed vertical line represents the glass transition temperature from DSC measurements. In rheological experiments T_g was obtained by the local maximum of G'' at a frequency of 0.01 rad/s.

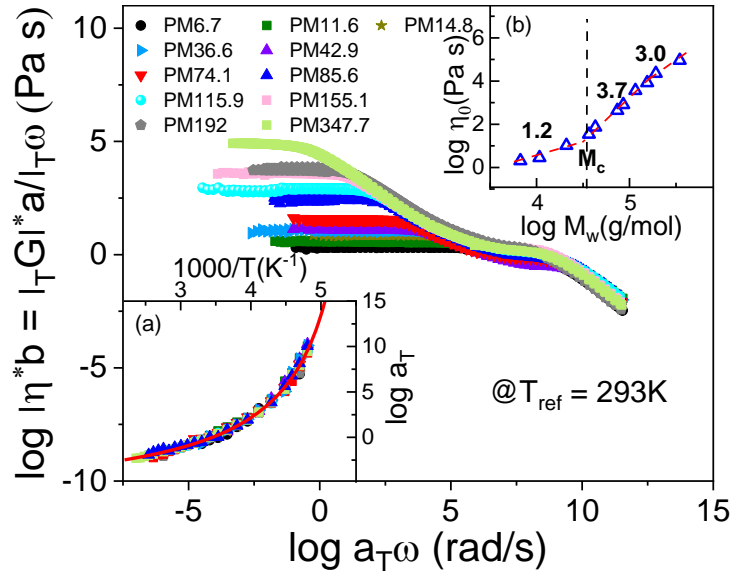


Figure 12: Complex viscosity versus reduced frequency for the PM samples at $T_{ref} = 293$ K. Insets: (a) Frequency shift factors (a_T) used to generate the master curves. The solid red line represents fits using the WLF equation and (b) Zero shear viscosities at $T_{ref} = 293$ K as a function of M_w for the PM materials. The dotted vertical line represent the approximate critical molecular weight $M_c \cong 4.4 \cdot 10^4$ g/mol for PM. Slope values are also indicated.

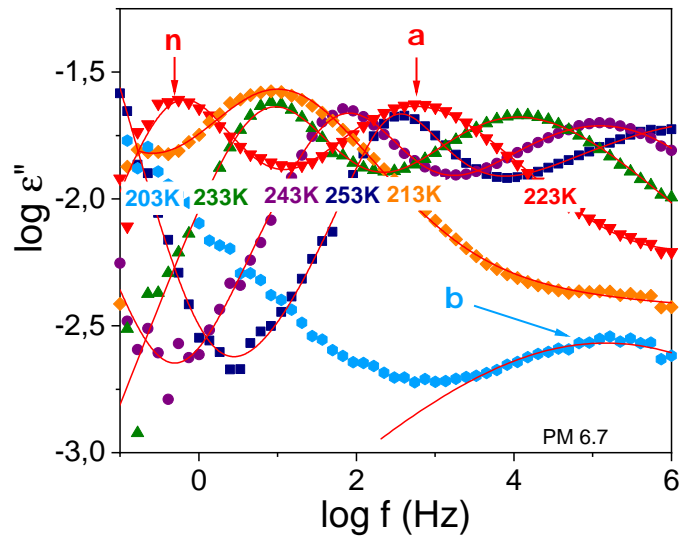


Figure 13: PM 6.7 dielectric loss spectra at selected temperatures as indicated versus frequency. Three relaxation processes are observed: The normal mode (n), the α -relaxation, and the β -relaxation. The solid lines represents the HN fits.

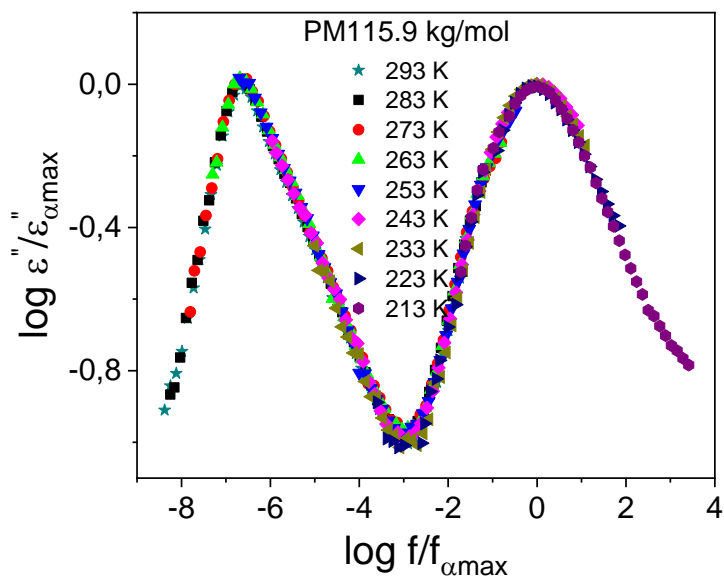


Figure 14: Rescaled dielectric spectra for PM 115.9 for indicated temperatures; where ϵ'' is rescaled by the maximum height $\epsilon''_{\alpha,max}$ and f by the frequency $f_{\alpha,max}$ of the α -peak.

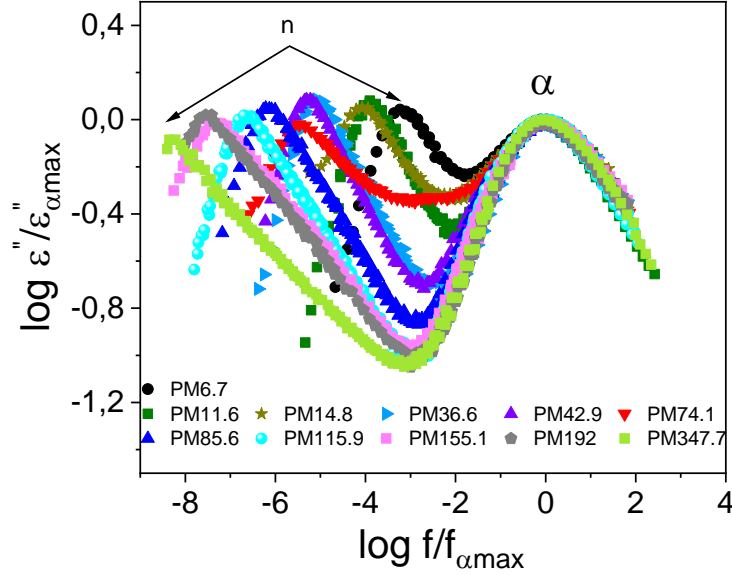


Figure 15: Rescaled dielectric spectra of polymyrcene samples investigated: PM6.7 (T=213-233K), PM11.6 (T=213-243K), PM14.8 (T=223-233K), PM36.6 (T=223-253K, PM42.9(T=233-253K), PM74.1 (T=233-263K), PM85.6 (T=243-273K), PM115.9 (T=233-293K), PM155.1 (T=263-283K), PM347.7 (T=273-293K): dielectric permittivity ϵ'' rescaled by its α -peak height $\epsilon''_{\alpha,max}$ and f rescaled by the frequency $f_{\alpha,max}$ of the α -peak.

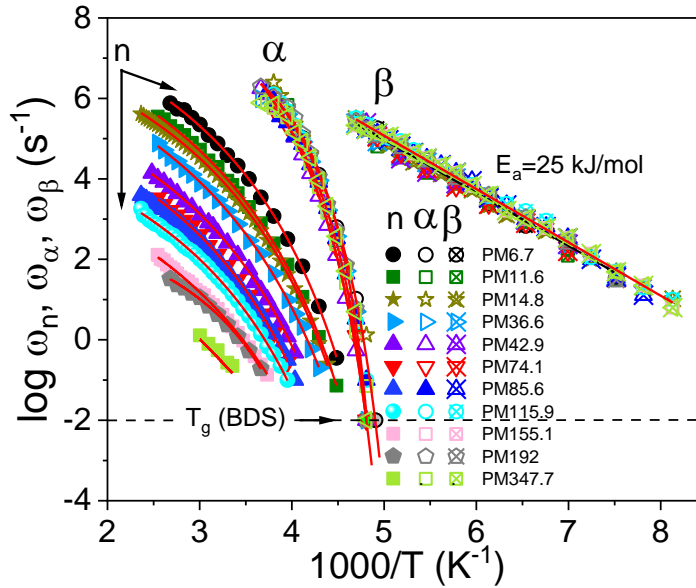


Figure 16: Relaxation rates for the glassy state β -relaxation, ω_β , the segmental relaxation process, ω_α and the normal mode relaxation, ω_n for PM with different M_w versus $1000/T$. The solid lines are VFT- and Arrhenius- fits. The dashed line labeled T_g (BDS) indicates the extrapolation of the VFT fits to $1/\omega = 100$ s. The VFT fit parameters are presented in Table 2 of the SI. The T_g values obtained from BDS measurements are similar to those from LVE and DSC within experimental uncertainty.

References

- (1) Imanishi, Y.; Adachi, K.; Kotaka, T. Further investigation of the dielectric normal mode process in undiluted *cis* -polyisoprene with narrow distribution of molecular weight. The Journal of Chemical Physics **1988**, 89, 7585–7592, DOI: 10.1063/1.455244.
- (2) Matsumiya, Y.; Watanabe, H.; Osaki, K. Comparison of Dielectric and Viscoelastic Relaxation Functions of *cis* -Polyisoprenes: Test of Tube Dilatation Molecular Picture. Macromolecules **2000**, 33, 499–506, DOI: 10.1021/ma991121q.
- (3) Sato, T.; Watanabe, H.; Osaki, K.; Yao, M.-L. Relaxation of Spherical Micellar Systems of Styrene–Isoprene Diblock Copolymers. 1. Linear Viscoelastic and Dielectric Behavior. Macromolecules **1996**, 29, 3881–3889, DOI: 10.1021/ma951843r.
- (4) Iacob, C.; Yoo, T.; Runt, J. Molecular Dynamics of Polyfarnesene. Macromolecules **2018**, 51, 4917–4922, DOI: 10.1021/acs.macromol.8b00851.
- (5) Unidad, H. J.; Goad, M. A.; Bras, A. R.; Zamponi, M.; Faust, R.; Allgaier, J.; Pyckhout-Hintzen, W.; Wischniewski, A.; Richter, D.; Fetters, L. J. Consequences of Increasing Packing Length on the Dynamics of Polymer Melts. Macromolecules **2015**, 48, 6638–6645, DOI: 10.1021/acs.macromol.5b00341.
- (6) Sarkar, P.; Bhowmick, A. K. Synthesis, characterization and properties of a bio-based elastomer: polymyrcene. RSC Adv. **2014**, 4, 61343–61354, DOI: 10.1039/C4RA09475A.
- (7) Abou Elfadl, A.; Kahlau, R.; Herrmann, A.; Novikov, V. N.; Rössler, E. A. From Rouse to Fully Established Entanglement Dynamics: A Study of Polyisoprene by Dielectric Spectroscopy. 43, 3340–3351, DOI: 10.1021/ma902564b.